Available online at www.sciencedirect.com
ScienceDirect
Developmental Biology 314 (2008) 261–275
DEVELOPMENTAL BIOLOGY
www.elsevier.com/developmentalbiology

Zebrafish mutations affecting cilia motility share similar cystic phenotypes and suggest a mechanism of cyst formation that differs from *pkd2* morphants

Jessica Sullivan-Brown [a], Jodi Schottenfeld [a], Noriko Okabe [a], Christine L. Hostetter [a], Fabrizio C. Serluca [b], Stephan Y. Thiberge [a], Rebecca D. Burdine [a,*]

[a] *Department of Molecular Biology, Princeton University, Washington Road, Mof 433, Princeton, NJ 08544, USA*
[b] *Novartis Institutes for Biomedical Research. Developmental and Molecular Pathways. Cambridge, MA 02139, USA*

Received for publication 27 July 2007; revised 16 November 2007; accepted 19 November 2007
Available online 3 December 2007

Abstract

Zebrafish are an attractive model for studying the earliest cellular defects occurring during renal cyst formation because its kidney (the pronephros) is simple and genes that cause cystic kidney diseases (CKD) in humans, cause pronephric dilations in zebrafish. By comparing phenotypes in three different mutants, *locke*, *swt* and *kurly*, we find that dilations occur prior to 48 hpf in the medial tubules, a location similar to where cysts form in some mammalian diseases. We demonstrate that the first observable phenotypes associated with dilation include cilia motility and luminal remodeling defects. Importantly, we show that some phenotypes common to human CKD, such as an increased number of cells, are secondary consequences of dilation. Despite having differences in cilia motility, *locke*, *swt* and *kurly* share similar cystic phenotypes, suggesting that they function in a common pathway. To begin to understand the molecular mechanisms involved in cyst formation, we have cloned the *swt* mutation and find that it encodes a novel leucine rich repeat containing protein (LRRC50), which is thought to function in correct dynein assembly in cilia. Finally, we show that knock-down of *polycystic kidney disease 2 (pkd2)* specifically causes glomerular cysts and does not affect cilia motility, suggesting multiple mechanisms exist for cyst formation.

Keywords: Pronephros; Cyst; Kidney; Zebrafish; Cilia; *locke*; *switch hitter*; *lrrc50*; *kurly*; *pkd2*; oda7; Nephron

Introduction

Renal cystic kidney diseases are pleiotrophic disorders that are clinically variable and genetically diverse. Depending on the type of disease, cysts can occur in different locations of the kidney and can present at various stages of life ranging from fetal development to adulthood. The most prevalent form of renal cystic disease is Autosomal Dominant Polycystic Kidney Disease (ADPKD), which can occur in 1:1000 individuals and is caused by mutations in the genes *PKD1* or *PKD2* (1994; 1995; Burn et al., 1995; Gabow, 1993). ADPKD is further associated with extra-renal pathologies such as liver cysts and cardiac deformities (Perrone, 1997). The onset of clinical symptoms begins later in adulthood and cysts have been shown to arise from all areas of the nephron, with a majority of focal cysts occurring in the collecting ducts (Baert, 1978; Verani and Silva, 1988). By contrast, Autosomal Recessive PKD (ARPKD) is rare, occurring in 1:20,000 live births, and cysts form mainly in the collecting ducts early in utero (Zerres et al., 1998). The pathological presentation of cysts in ARPKD shows fusiform dilations, while in ADPKD the cysts are focally derived and bud from the epithelium (Wilson, 2004). ARPKD is caused by mutations in the gene fibrocystin (*PKHD1*), which is also associated with congenital defects in the liver (Onuchic et al., 2002; Ward et al., 2002). Nephronophthisis disorders are characterized by renal cysts occurring in the corticomedullary junction of the kidney, which present later during childhood or early adulthood (Hildebrandt and Zhou, 2007). Bardet–Biel Syndrome is associated with a number of clinical presentations

* Corresponding author. Fax: +1 609 258 1343.
E-mail address: rburdine@princeton.edu (R.D. Burdine).

0012-1606/$ - see front matter © 2007 Elsevier Inc. All rights reserved.
doi:10.1016/j.ydbio.2007.11.025

such as retinal degeneration, obesity, polydactyly and in some cases renal cysts (Blacque and Leroux, 2006). Despite the diversity of these syndromes, the majority of gene products mutated in each of these cases are known to associate with the cilium, centrosome or basal bodies (reviewed in Torres and Harris, 2006). The discoveries that these diseases stem from a functional or structural defect related to cilia are so prevalent that these groups of disorders have been collectively described as "ciliopathies" (Badano et al., 2006; Hildebrandt and Zhou, 2007).

Although the location and timing of cyst development vary in different disease states, the cellular defects observed in renal cysts are similar. Cystic dilations are characterized by increased cellular proliferation and increased fluid secretion possibly due to the apical mistargeting of ion channel proteins like the Na^+/K^+ATPase or EGFR/ErbB2 heterodimers (reviewed in Wilson, 2004). Since the majority of proteins known to be involved in renal cystic diseases are found associated with the cilium, much research has been focused on uncovering the physiological significance of this (once thought to be vestigial) organelle. The mechanosensory hypothesis is the most common functional role assigned to renal cilia, in which the physical bending of cilia results in the elevation of cytoplasmic calcium concentrations (Praetorius et al., 2003; Praetorius and Spring, 2001). It is thought that this rise in calcium could participate in cellular signaling events that are critical for tubular integrity. Defects in cilia may prevent these processes, leading to unregulated cell growth and a less differentiated epithelium.

The zebrafish pronephros provides an attractive model system for studying cyst formation at the cellular level. The pronephros is the first kidney to form in all vertebrates and is replaced by a more advanced kidney in mammals (Vize et al., 1997). Although the pronephros in mammals is thought to be nonfunctional, the pronephros in zebrafish is active, acts as a closed system, and mimics mammalian kidneys in terms of gene expression and maintaining osmotic homeostasis (Drummond et al., 1998). In essence, the pronephros is a simple version of the more advanced mammalian kidney. The functional unit of the pronephros is termed the nephron and is composed of two tubules connecting to a fused glomerulus. The glomerulus functions as the site of filtration, where hydrostatic pressure from the capillaries and the glomerular capsule work to force fluid, salts and other small inorganic molecules nonselectively into Bowman's space. The tubules and ducts are generally composed of highly reabsorptive cells that further refine the filtrate by allowing ions and salts back into the blood. The zebrafish pronephros forms very early in development, as cells fated to become the glomerulus, tubules and ducts are specified by the 8 somite stage (12 hours post-fertilization (hpf)) (Serluca and Fishman, 2001). Similar to the mammalian system, expression of *wt1* (*wilm's tumor 1*) marks the glomerular fated tissue and *pax2.1* marks the tubule and duct precursors (Serluca and Fishman, 2001). By 24 hpf the glomerular fated tissue, which began as bilateral progenitor populations on either side of midline, migrates to the midline and fuses at 50 hpf (Drummond et al., 1998). Glomerular filtration begins between 36 and 48 hpf as evidenced by injecting rhodamine dextran into the circulatory system and monitoring when the dye first appears in the pronephric lumen (Drummond et al., 1998). Thus, the zebrafish pronephros develops quickly, and with a simple anatomy, allowing for earlier phenotypes to be more easily addressed.

In the zebrafish pronephros, cilia lining the tubules and ducts differ from mammalian renal cilia. Cells of the pronephros show a "salt and pepper" array of both single ciliated cells and multiciliated cells (Liu et al., 2007; Ma and Jiang, 2007). The cilia on the multiciliated cells have a 9+2 microtubule arrangement, a striking difference from mammalian tubules which possess immotile 9+0 cilia. Furthermore, cilia in the zebrafish pronephros, and in the pronephros of other fish species, are motile and this motility is thought to be important for moving fluid through the kidney (Kramer-Zucker et al., 2005; Lacy et al., 1989). It has been shown by other laboratories that cilia motility is affected in the cystic kidneys of zebrafish at 2–3 days post-fertilization (dpf) (Kramer-Zucker et al., 2005; Omori and Malicki, 2006). Despite these differences, the prevalence of ciliary defects related to cystic kidney phenotypes is highly conserved from mammals to teleosts.

Here we provide a detailed analysis of the spatial and temporal progression of pronephric cyst development in zebrafish in three mutants with cilia motility defects; *locke*, *switch hitter (swt)* and *kurly*. From this time course, our results indicate that cystic dilations occur first in the medial region of the pronephric tubules and may involve defects in luminal remodeling. This is in contrast to the *pkd2* morphant, in which the dilation is restricted to the glomerular region. Furthermore, we uncovered different functional roles of each gene product in regulating ciliogenesis or cilia motility that precede or act in parallel to cystic expansion. We have cloned the *swt* mutation to a gene encoding a novel leucine rich repeat containing protein (LRRC50) which is expressed in tissues that contain motile cilia. By undertaking this time course of cyst formation in the zebrafish, we provide the foundation to further understand the primary cause of tubular dilation, better characterize the cellular defects occurring in cystic cells and study ciliary defects related to cystogenesis.

Materials and methods

Zebrafish strains

locke (to237b), *switch hitter* (*tm317*) and *kurly* (*tm304*) were obtained from a large scale ENU mutagenesis screen (Brand et al., 1996; Haffter et al., 1996). *locke*, *switch hitter*^{tm317} and *kurly* alleles were generated in the Tü strain and maintained by outcrossing to AB, WIK and PWT. *switch hitter*^{fk03a} was isolated in a recessive genetic screen for visual kidney defects. The mutant allele was generated in the TL background and crossed to the WIK line to generate heterozyous mapping pairs. The kidney phenotypes associated with each allele have been observed across multiple generations. Embryos were collected and raised per standard protocols.

switch hitter positional cloning

The *swt* locus was mapped using SSLP markers (Liao and Zon, 1999). The *swt* genomic interval was narrowed between markers z11119 and z15270 on chromosome 7, where *lrrc50* was identified as a candidate gene. To identify mutations, we amplified each exon from mutant genomic DNA and compared the sequences obtained with wild-type siblings and Tü sequence.

Histology

Embryos were fixed in 4% paraformaldehyde (PFA; Sigma P6148)/Phosphate Buffered Saline (PBS) overnight at 4 °C. After gradual dehydration into ethanol, embryos were infiltrated and embedded in JB-4 plastic resin (JB-4 Embedding Kit, EMS #14270-00) according to the protocol provided by Electron Microscopy Sciences. All embryos were sectioned at 4 μm on a Leica RM2255 Rotary Microtome. Sections were then stained with hematoxylin and eosin dyes according to our standard laboratory protocols (available upon request).

Counting cell number

To perform this analysis, embryos were sectioned in a transverse orientation at 4 μm in JB-4 plastic resin. Sections were collected in consecutive order and stained with hematoxylin and eosin which readily distinguishes nuclei for counting. We counted nuclei in 15 consecutive sections (roughly 60 μm) from the glomerular/anterior region and medial region of the kidney. The start of the glomerular/anterior region began when both the glomerulus and a cross-section through a tubule were observed in the same section, and ended in the anterior tubular region (Figs. 2B, C). The medial tubule sections were defined as a point posterior to the visceral organs where the gut had migrated toward the middle of the body (Fig. 2D). Cells were counted from the anterior region at 2 dpf and 3 dpf. We did not count kidney cells in the anterior region at later time points because the tubules extending from the glomerulus become convoluted, making the analysis inconsistent.

Immunofluorescence

Staining for F-actin was performed on cryosections. Embryos were fixed in 4% PFA at 4 °C overnight, washed once with PBS, and soaked in 10% sucrose/PBS at 4 °C until the embryos sank to the bottom of the epitube. Next, embryos were soaked in 25% sucrose/PBS at 4 °C until the embryos sank. Embryos were then embedded in Tissue-Tek® O.C.T. compound which was allowed to solidify on dry ice. The embryos were sectioned at 8 μm using the Leica CM 3050S. Sections were washed in PBS with 0.005% saponin (PBS-saponin) twice and blocked in 5% normal goat serum (NGS) in PBS-saponin at room temperature for 30 min. Samples were incubated with rhodamine-phalloidin at room temperature for 1 h. After washing three times for 20 min each, samples were equilibrated in 50% glycerol/PBS.

ZO-1 and Na^+/K^+ATPase stainings were performed in whole mount embryos, then embedded and sectioned in JB-4 plastic resin. Embryos were fixed in Dent's solution (80% MeOH; 20% DMSO) overnight at 4 °C. Embryos were slowly rehydrated into PBDT (1% DMSO, 0.1% Tween 20/PBS) and blocked for 2 h in PBDT containing 10% NGS. Antibodies to ZO-1 (Zymed) and Na^+/K^+ATPase (α6F; Developmental Studies Hybridoma Bank, U. of Iowa) were added at a 1:200 and 1:25 concentration, respectively. Primary antibodies were added at 4 °C overnight. Samples were washed 5 times, 30 min each wash in 1%NGS/PBDT. ZO-1 was detected using the secondary antibody FITC goat anti-mouse IgG_1 (Southern BioTech, Birmingham, AL) and the Na^+/K^+ATPase was detected using Alexa Fluor® 568 goat anti-mouse IgG_{2a} antibody, both at a concentration of 1:500. To visualize the nuclei, Hoechst dye was added with the secondary antibody at a 12.96 μM concentration overnight. The next day, embryos were washed with 1% NGS/PBDT buffer for 5 times, 30 min each wash. Embryos were embedded according to the JB-4 histology protocol provided by the manufacturer; however, the dehydration steps were performed quickly and the embedding steps were performed at 4 °C. Sections were collected at 4 μm. Both cryosection and JB-4 plastic sections were coverslipped in a 50% glycerol/PBS solution and imaged with a ZEISS LSM 510 confocal microscope.

The acetylated tubulin immunostaining was performed on embryos fixed either in Dent's or 4% PFA overnight. All staining procedures were performed in whole mount in a manner similar to the protocol mentioned above. The anti-acetylated tubulin antibody (Sigma #T6793) was added at a concentration of 1:400 and the goat anti-mouse IgG_{2b} secondary antibody (Southern BioTech, Birmingham, AL) was added at a concentration of 1:500. Embryos were mounted and imaged in AquaPolyMount (Polysciences, Inc., Warrington, PA) with a ZEISS LSM510 confocal microscope.

Video microscopy

Embryos were rinsed in double distilled H_2O to remove any residual methlylene blue or salts from the embryo medium. A glass depression slide (Ward's Natural Science) was prepared by filling the depression with 3% methylcellulose (Sigma M-0387) and 2 drops of 0.4% Tricaine (MS-222; Sigma A-5040). Embryos were oriented along their lateral sides and cilia motility was recorded starting in the cloaca and posterior regions (data not shown). We continued imaging the tubule from posterior to anterior until we reached the medial segments. All movies shown were recorded in the medial segments. The tubules were imaged with an Olympus BX51 up-right microscope equipped with a 60× water immersion objective and differential interference contrast (DIC) optics. Video was recorded with an iXon camera (Andor Technology) and Luca camera (Andor Technology). The Luca camera incorporates frame transfer technology which allows relatively fast image acquisition. We recorded movies with the iXon camera between 10 and 20 frames per second (fps) and with the Luca camera at 158 fps. All movies were slowed down to 8 fps, except Supplementary Video 3 which was slowed to 15 fps.

Cilia frequency measurements

As frequency measurements obtained from movie analysis could be impaired by a low frame rate, we built a specialized set-up to perform high precision cilia frequency measurements. A shutter controlled infra-red laser beam at 900 nm, entering the microscope, was focused on the cilia and a small portion of the scattered light was collected by an optical fiber connected to an avalanche photodiode. As the cilia moves in and out of the focused beam during the periodic movement, the amount of scattered light entering the fiber varies accordingly. The entrance of the fiber was brought to close proximity of the fish (~1 mm). The detector output was recorded for several seconds with a sampling rate of one millisecond. Finally, a Fourier transform analysis of the recorded trace was made using Matlab to uncover the frequency content of the data. While the beam was focused on the cilia, the frequency spectrum revealed very sharp peaks that disappeared when focusing the laser elsewhere in the animal. Care was taken to use low laser intensity. We found that 10 mW power entering the back aperture of the objective was sufficient for high signal collection and harmless to the animal. As we could not appreciate any systematic variation of the cilia frequency over the time the shutter was opened, we concluded the laser has no indirect effect on the cilia movement.

RNA whole-mount in situ hybridization

DIG-labeled RNA probes were used in RNA in situ hybridization using standard methods. The *swt* cDNA was amplified from a zebrafish 24 hpf cDNA library and cloned into Bluescript KS (Stratagene). For the sense probe, the plasmid was linearized with *Kpn*I and transcribed with T3 enzyme and for the antisense probe the plasmid was linearized with *Sac*I and transcribed with T7 enzyme.

Results

locke, switch hitter and kurly mutants develop pronephric cysts

locke, *switch hitter* (*swt*) and *kurly* mutants were originally generated in the Tübingen mutagenesis screen as recessive mutations that displayed a "curly tail down" phenotype and developed cystic dilations in the pronephros (Brand et al., 1996; Haffter et al., 1996).

The curly tail phenotype is not linked to the development of pronephric cysts, as some mutants with a curly tail down phenotype do not develop pronephric dilations (Brand et al., 1996, and JSB-personal observations). The curly tail down phenotype is first observed at 26 hpf, which is the

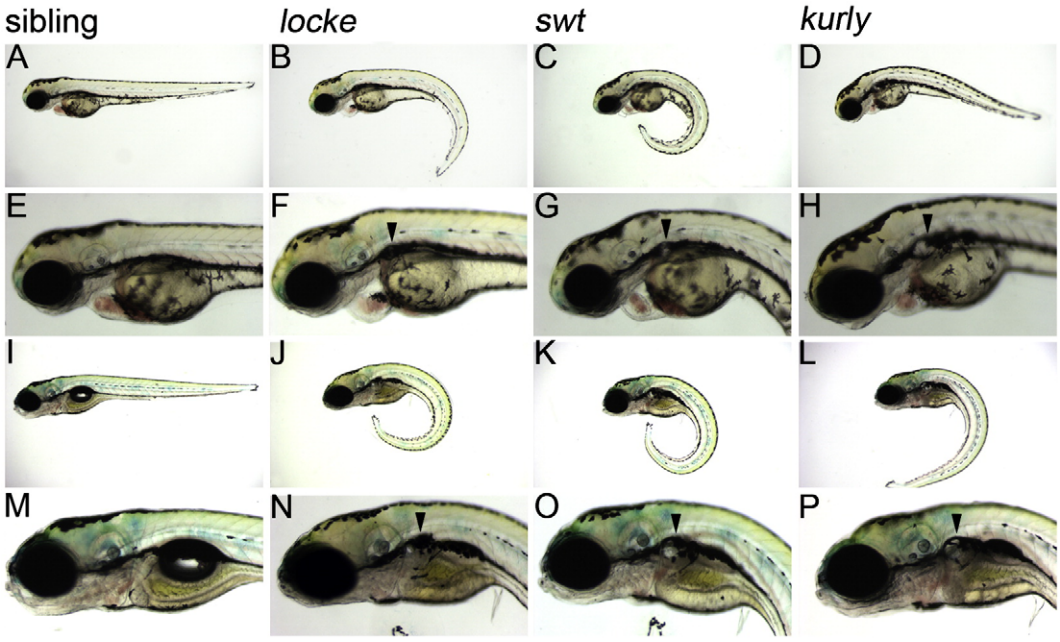

Fig. 1. *locke*, *swt* and *kurly* mutants develop pronephric cysts. (A–H) 3 dpf, (I–P) 5 dpf. At 3 dpf, *locke*, *swt* and *kurly* mutants are easily identified by their "curly-tail down" phenotype. Panels E–H are higher magnification images of panels A–D, showing the cystic dilations visible under light microscopy. At 5 dpf, the cystic dilations have increased in size shown in panels I–L and magnified in panels M–P. The black arrowheads mark the location of the cysts, posterior to the eye and ear. In general, *locke* mutants have smaller cysts than *swt* or *kurly*.

first time point where we can morphologically distinguish the mutants from their siblings. By 3 dpf, both *locke* and *swt* exhibit a strong downward curve in their body axis; however, the phenotype observed in *kurly* mutants is less severe (Figs. 1A–H). At 3 dpf, cystic dilations are observable by light microscopy in a region slightly posterior to the ear, shown by the black arrowheads. By 5 dpf, the cystic dilations have increased in size (Figs. 1I–P). Although the size of the cysts varies in mutants from the same clutch, *swt* and *kurly* mutants tend to develop larger cysts than *locke* mutant embryos. Despite their cystic developments, *locke*, *swt* and *kurly* mutants rarely become grossly edemic. Because edema is a hallmark sign of glomerular filtration failure, we believe that the kidneys are functioning in these mutant embryos.

Cystic dilations first appear in the medial tubules in locke, swt and kurly mutants

The temporal and spatial development of pronephric cystic phenotypes was assessed by performing a histological time course. Fig. 2 shows representative histological sections of a 2 dpf wild-type embryo, highlighting different regions of the pronephros along the anterior to posterior axis. Throughout the text, we will be referring to 5 distinct regions; the glomerulus, anterior tubules, medial tubules, posterior tubules and the cloaca region (Fig. 2). Cystic dilations are first observed under simple light microscopy in the glomerular region at 2.5 dpf. However, we can detect earlier tubular dilation by histology and DIC at 2 dpf. At 2 dpf, the medial tubules are clearly dilated in all embryos examined as evidenced by histology (Figs. 3E–H). Interestingly, in these mutants, the glomerular region and posterior portions of the kidney appear normal (Figs. 3A–D, data not shown). Although some embryos have begun to develop dilations in the glomerulus around 2 dpf, this is always accompanied by dilations in the medial tubular region. These cystic dilations appear fusiform in nature, as they are wider at a specific area of the kidney and tapered at either end. This is similar architecture to that observed in ARPKD cysts (Menezes and Onuchic, 2006). We first consistently observe glomerular dilations at 2.5 dpf which progress over time (Figs. 3I–L). Increased filtrate volumes into Bowman's capsule are clearly evident, causing a disorganization of the capillaries and the associated podocytes. The extended glomerulus is observed both along the proximal–distal axis and anterior–posterior axis. Although the medial tubules continue to become dilated (Figs. 3M–P), the more posterior tubules are less affected, approaching the size of the wild-type tubules (Figs. 3Q–T). Cloaca development in *locke*, *swt* and *kurly* mutants appears normal, as the two pronephric ducts fuse in the posterior segment of the kidney and the lumen remains intact (data not shown). By performing this histological time course, we find that dilations first occur by 2 dpf in the medial tubules which are analogous to the proximal convoluted and straight tubules in higher vertebrates (Wingert et al., 2007), a region where dilations are observed in PKD.

Increased number of cells around the cystic kidney tubules is secondary to dilation

Increased cell proliferation is a characteristic trait of nephron dilation in mammalian renal cystic diseases (Nadasdy et al., 1995; Ramasubbu et al., 1998). Since cell proliferation has not

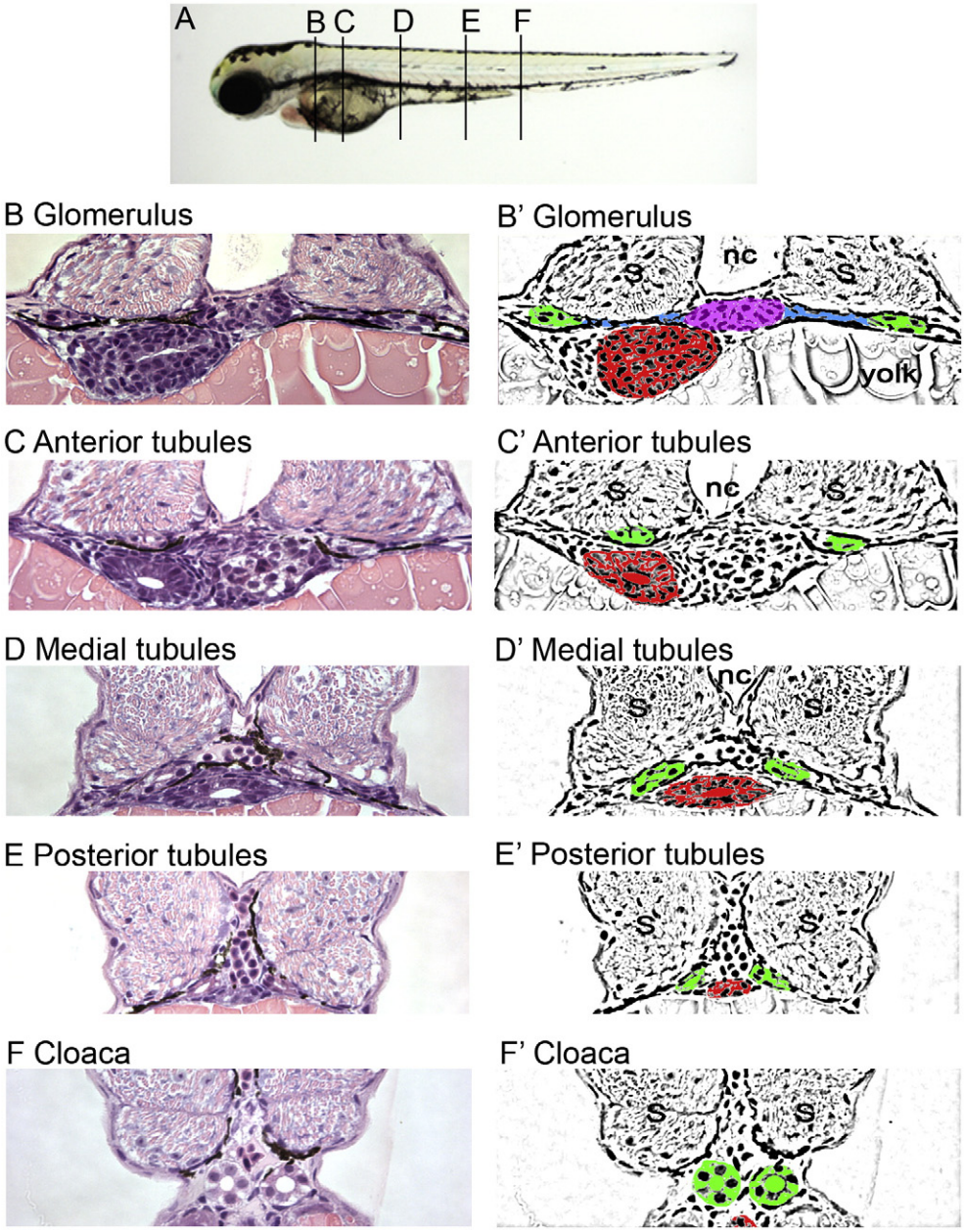

Fig. 2. Histological and schematic representations of the pronephros along the anterior to posterior axis. (A) Depiction of the corresponding regions referred to in the text. (B, C, D, E, F) Histological sections stained with hematoxylin and eosin. Pictures taken with a 40× objective lens. (B′, C′, D′, E′, F′) Schematic diagrams highlighting regions of interest. (B, B′) Glomerulus: The glomerulus (pink) is found ventral to the notochord (nc) and medial to either somite (s). Connecting to the glomerulus are tubules that extend laterally (blue). The tubules then turn at the edge of the somites and extend toward the posterior (green). Also shown is the gut (red). (C, C′) Anterior tubules: The region designated as the anterior tubules is slightly posterior to the glomerulus region in which the viscera can be observed. (D, D′) Medial tubules: In this region, the gut (red) and tubules (green) are positioned toward the midline and ventral to the notochord (nc). (E, E′) Posterior tubules: The gut has become smaller and the tubules (green) are positioned more medially. (F, F′) Cloaca: This is the most posterior section before the tubules fuse into a single opening outside the body.

been examined in zebrafish pronephric cyst formation, we determined whether there were increased numbers of cells surrounding mutant pronephric tubules. Data collected at 2 dpf did not show a significant difference in cell number in the glomerular/anterior region (Fig. 4). However, by 3 dpf, *locke* and *kurly* showed an increase in cell number surrounding the tubules. The anterior region at 5 dpf could not be examined because the pronephric tubules become convoluted. The medial region of the kidney was then examined at 2 dpf, 3 dpf and 5 dpf. At 2 dpf, all mutants showed dilations in the medial region; however, the cell number surrounding the kidney tubule was not statistically significant from the wild-type tubules. By 3 dpf, there was a significant increase in cell number when compared to the wild-type tubules which became more pronounced at 5 dpf (Table 1 and Fig. 4). This is the first time an increased number of cells surrounding cystic mutant tubules have been reported in zebrafish. However, this increase occurs after the tubules have become dilated (see above) and

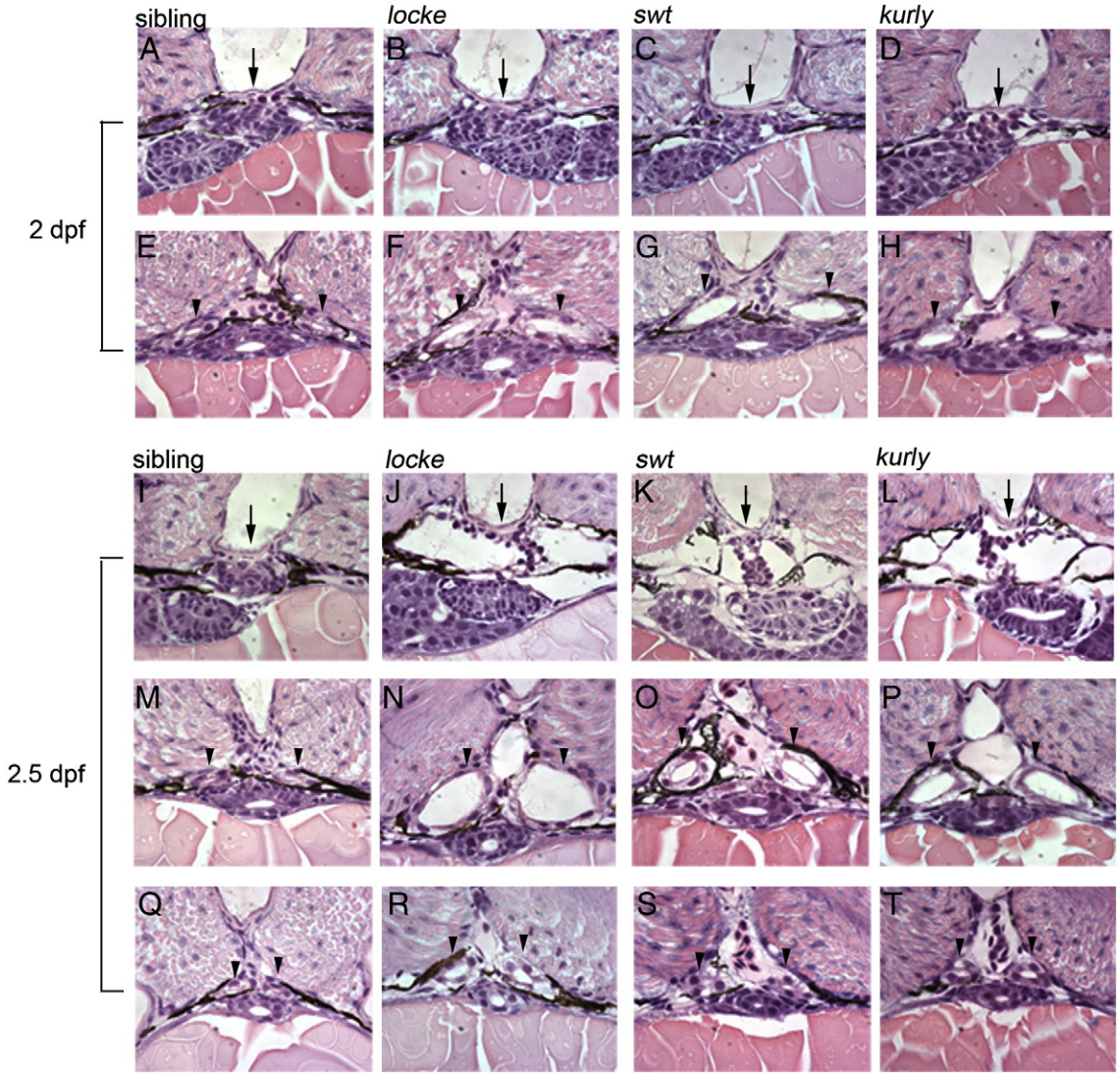

Fig. 3. Temporal and spatial analysis of cystic kidneys in zebrafish mutants. (A–H) 2 dpf; (I–T) 2.5 dpf. At 2 dpf, the glomerulus (arrows, A–D) appears intact in the mutant embryos; however, the medial tubules have become dilated (arrowheads, E–H). At 2.5 dpf, the glomerulus (arrows, I–L) and surrounding Bowman's space have become enlarged, compressing the podocytes in the mutants. The medial tubules are grossly dilated (arrowheads, M–P). Interestingly, the posterior tubules are less dilated, approaching wild-type size (arrowheads, Q–T). All pictures are 4 μm JB-4 plastic sections, stained with hematoxylin and eosin and taken with a 100× oil objective lens.

indicates that an increase in cell number is a secondary effect and not the primary cause of cyst formation in zebrafish.

Pronephric lumen size decreases over time in wild-type embryos, while mutant lumen size increases

As stated previously, we first observe cystic dilations in the medial tubules by 48 hpf through histology and DIC microscopy. At earlier time points (26–30 hpf), we found that the wild-type medial tubules had a larger luminal diameter compared to the posterior tubules (Figs. 5E, G). Over time, the lumen size in the medial tubules of wild-type embryos decreases, which is supported by our observation of decreased cell number surrounding the medial tubules from 2 dpf to 3–5 dpf (Fig. 4 and Table 1).

When mutant embryos were examined at 26–30 hpf, the size of the medial and posterior tubule lumens was similar to wild-type (Figs. 5F and H). However, in mutant embryos, there is a consistent increase in the medial lumen diameter size by 48 hpf when compared to wild-type tubule lumens (Figs. 5I, J). These data suggest that wild-type tubules undergo a remodeling process to refine tubule size, and that these processes are affected in the mutant tubules.

Localization of the Na^+/K^+ATPase is disrupted in mutant kidney cells, while apical polarity is intact

Cysts are classically defined as fluid-filled cavities lined by an epithelium. As observed in Fig. 3, the cells lining the cysts have altered morphology and often appear flattened. Therefore, we sought to determine if epithelial polarity is affected in *locke*, *swt* and *kurly* mutant embryos by staining for F-actin and the tight junction marker ZO-1. At 2 dpf, cystic expansions have begun in the medial positions of the kidney; however, F-actin

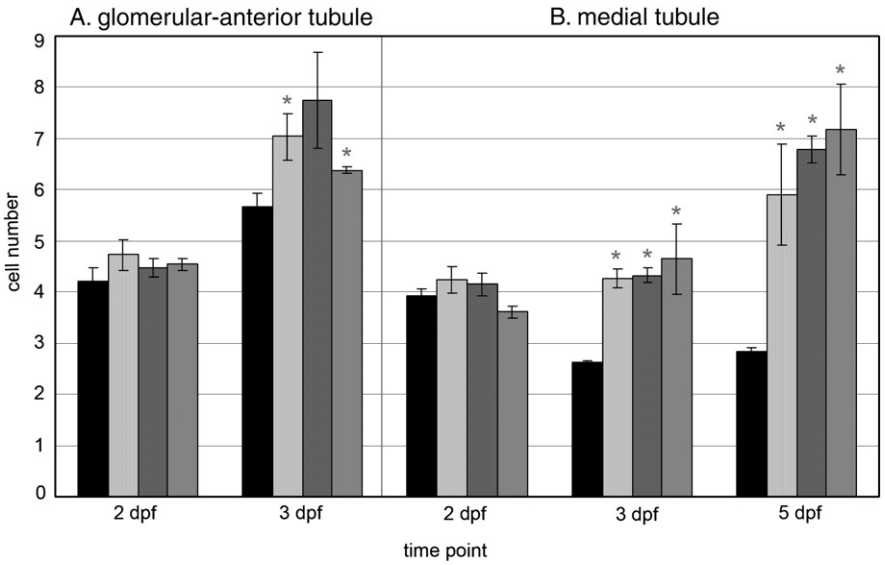

Fig. 4. Average cell number surrounding the medial tubules in the mutant backgrounds is increased at 3 dpf. (A) Bar graphs display the average cell number surrounding the glomerular-anterior tubule lumen at 2 dpf and 3 dpf. At 2 dpf, there is no significant increase in cell number surrounding the tubules between wild-type sibling and mutant populations. However, at 3 dpf, there is a statistical difference in cell number in *locke* and *kurly* mutant embryos. (B) Bar graphs depict the average cell number surrounding the medial tubule lumen at 2 dpf, 3 dpf and 5 dpf. At 2 dpf, there is no significant increase in cell number between the wild-type sibling and mutant populations. However, at 3 dpf and 5 dpf, the number of cells surrounding the lumen is significantly increased when compared to wild-type siblings. Interestingly, the number of cells in the wild-type sibling population decreases from 2 dpf to 5 dpf. In all graphs, the error bars represent standard error. Color code: black bars (sibling), light gray (*locke*), dark gray (*swt*) and medium gray (*kurly*).

and ZO-1 localization in these cells appeared normal (Figs. 6A–D and data not shown). At 4 dpf, although the tubules are largely expanded, the localization of F-actin and ZO-1 surrounding the kidney tubules at the apical surface remained normal (Figs. 6E–H and data not shown). The dedifferentiation of renal cells from a highly absorptive state to a secretory state is thought to be a leading factor in cystic fluid accumulation (Thomson et al., 2003). Some studies in mammals and zebrafish have shown that the Na^+/K^+ATPase is mistargeted to the apical surface of renal cystic cells, where secretion of sodium into the lumen can result in fluid accumulation (Avner et al., 1992; Drummond, 2003; Wilson et al., 2000). However, this theory is controversial, and other studies involving both human and mouse cystic tissue failed to show altered polarity of the Na^+/K^+ATPase (Brill et al., 1996; Thomson et al., 2003). Therefore, we sought to determine if the Na^+/K^+ATPase was mislocalized to the apical surface in *locke*, *swt* and *kurly* mutant embryos. We analyzed Na^+/K^+ATPase localization at 4 dpf in the anterior tubules, as this location showed the clearest basolateral staining in wild-type embryos. In *locke*, *swt* and *kurly* mutants, Na^+/K^+ATPase localization was significantly altered as the strict basolateral staining observed in the wild-type tubules was not evident. In some cells, apical expression of the Na^+/K^+ATPase was also observed (Figs. 6I, L, white arrows). Because the cells at this time point have abnormal morphology, we believe the defects in Na^+/K^+ATPase localization are secondary to increased fluid secretion in the tubules. Furthermore, in *kurly* mutant embryos, we did observe correct basolateral localization of the Na^+/K^+ATPase at 30 hpf, before tubule dilation begins (data not shown).

Cilia motility is affected prior to tubule dilation in locke, swt and kurly mutants

The connection of ciliary defects, whether structural or functional, with renal cystic diseases has been repeatedly established. However, we wanted to determine if cilia motility was affected prior to tubule dilation. We found that *locke*, *swt* and *kurly* mutants have unique cilia motility defects at 26–

Table 1

	Glomerular-anterior tubules		
	2 dpf	3 dpf	
Sibling	4.22±0.26 *n*=5 (3)	5.67±0.25 *n*=5 (3)	
locke	4.73±0.30 *n*=9 (6)	7.04±0.46 *n*=7 (4)*	
swt	4.47±0.18 *n*=7 (5)	7.75±0.94 *n*=7 (4)	
kurly	4.54±0.11 *n*=9 (5)	6.38±0.06 *n*=4 (4)*	
	Medial tubules		
	2 dpf	3 dpf	5 dpf
Sibling	3.94±0.12 *n*=6 (3)	2.64±0.01 *n*=7 (4)*	2.83±0.08 *n*=4 (2)*
locke	4.25±0.26 *n*=11 (6)	4.27±0.19 *n*=8 (4)*	5.90±0.99 *n*=4 (2)*
swt	4.15±0.22 *n*=8 (4)	4.33±0.15 *n*=6 (3)*	6.79±0.26 *n*=4 (2)*
kurly	3.61±0.12 *n*=10 (5)	4.65±0.69 *n*=6 (3)*	7.18±0.89 *n*=4 (2)*

These data points are displayed in the bar graphs in Fig. 4 and represent the means followed by standard error. The sample size (*n*) refers to the number of tubules used for this statistical analysis. The number in parenthesis refers to the total number of embryos used to generate the sample size. Although each embryo contains two tubules, in some embryos both of the tubules could not be accurately scored due to an incorrect position when sectioning. Asterisks (*) indicate that the difference between cell number in wild-type siblings and mutant embryos is statistically significant by Student's *t*-test (p-value<0.05).

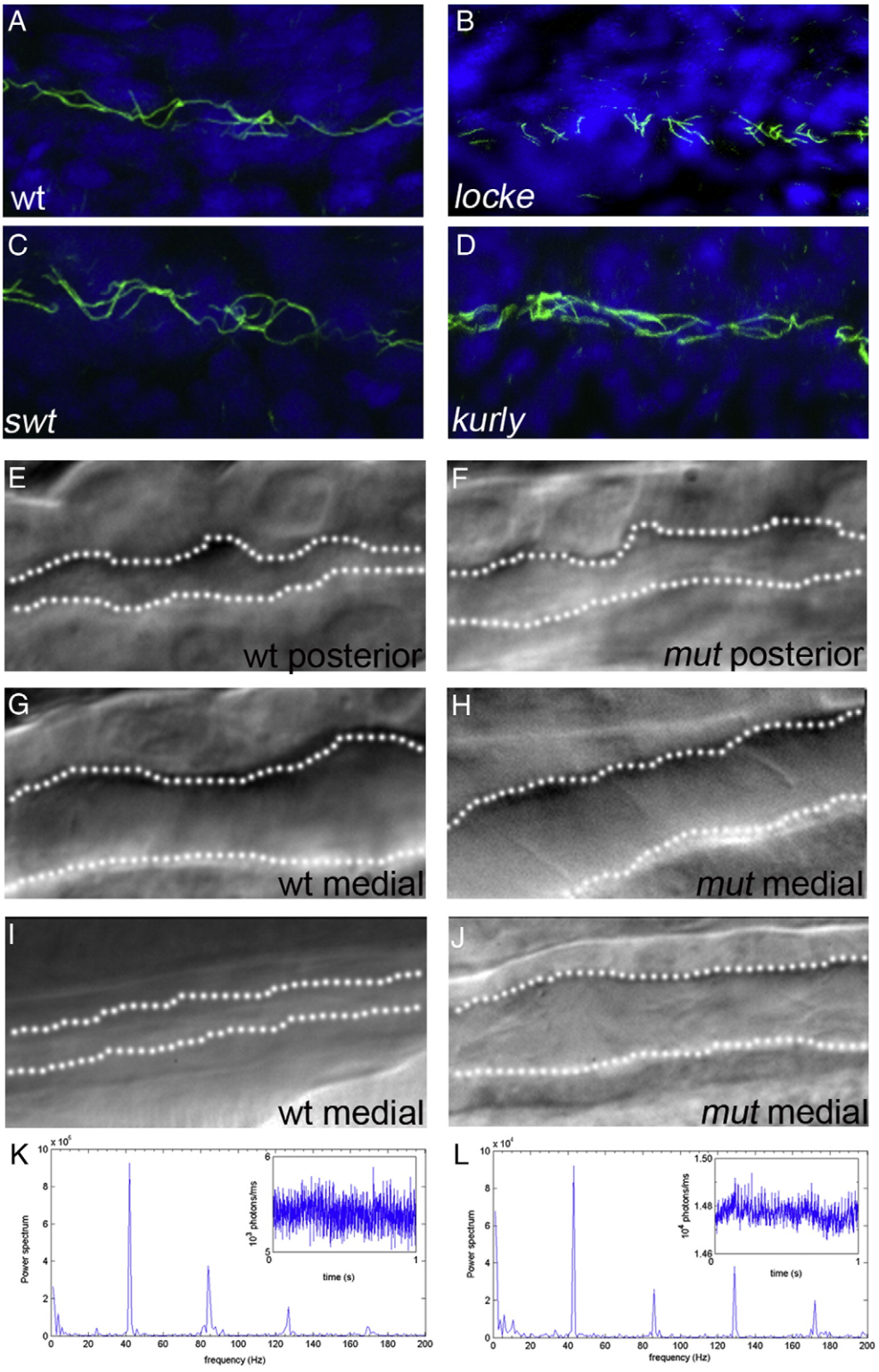

Fig. 5. Early pronephric cyst phenotypes. (A–D) Acetylated tubulin staining in the pronephric tubules at 27 hpf. Cilia were detected using an anti-acetylated tubulin antibody (green) and counterstained with the nuclear marker Hoechst (blue). Cilia appeared grossly normal in *swt* and *kurly*, but are shorter in *locke* when compared to wild-type siblings. (E–J) DIC microscopy images of the pronephric tubules in wild-type siblings and *kurly* mutants. Lumen sizes in posterior tubules from 26–30 hpf are similar in both wild-type siblings (E) and mutant embryos (F). Lumens in the medial tubules are larger in both wild-type siblings (G) and mutant embryos (H) when compared in the posterior regions (E, F). By 2 dpf, there is a clear dilation in the medial tubules of mutant embryos (J) as compared to wild-type siblings (I). (K, L) Infra-red scattering measurements demonstrate that the frequency of cilia movement in *kurly* mutants (L) is similar to the frequency observed in wild-type sibling embryos (K) (~42 Hz). Both spectra show several peaks. The first peak in each spectrum corresponds to the fundamental frequency of cilia movement. The subsequent peaks corresponds to the harmonics of the fundamental frequency (~n*42 Hz with n=1, 2 and 3). Panels E–J were taken with a 60× objective water immersion lens using two different cameras. Panels E–H were taken with an iXon camera (Andor); pixel size 16*16 μm. Panels I and J were taken with a Luca camera (Andor); pixel size of 10*10 μm. Because of differences in pixel size, luminal size in panels E–H cannot be directly compared to panels I and J.

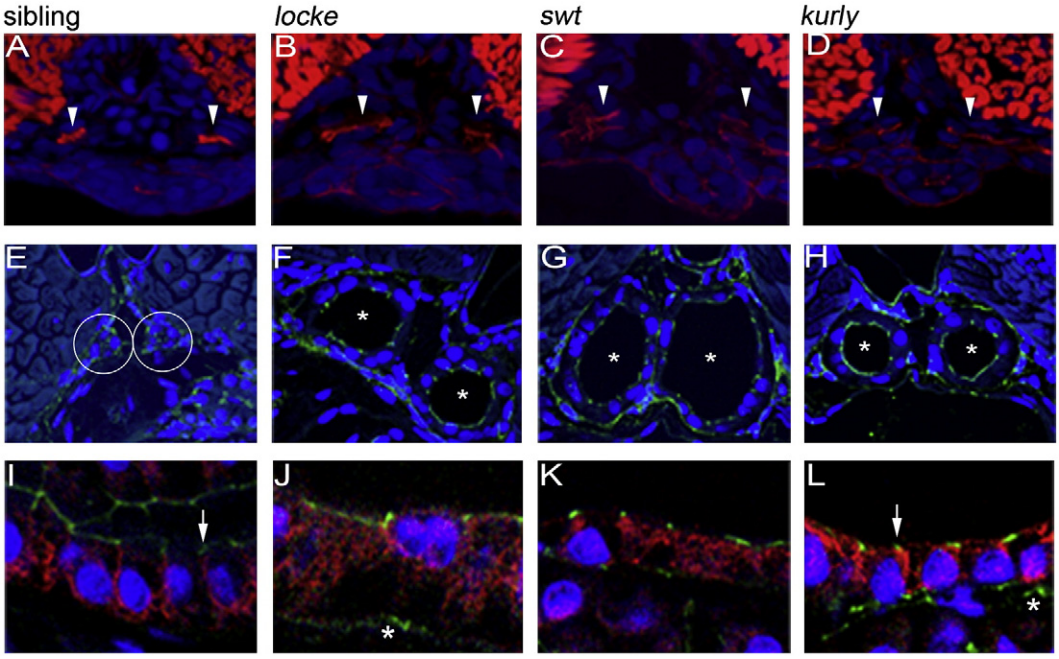

Fig. 6. Na^+/K^+ATPase localization is disrupted in cystic tissues, while apical polarity is maintained. Apical localization of F-actin (red) observed in 2 dpf wild-type siblings (A) is maintained in the medial tubules (white arrowheads) of mutants (B–D). The somites and gut are also stained by phalloidin (red). Correct apical localization of ZO-1 (green) is observed in 4 dpf wild-type sibling (E) and mutant (F–H) embryos. Sibling tubules are outlined by a white circle, and mutant tubules are distinguished by asterisks. Basolateral localization of the Na^+/K^+ATPase (red) observed in wild-type siblings (I) is altered in cystic mutants at 4 dpf (J–L). Note in panels J–L that Na^+/K^+ATPase is adjacent to apical ZO-1 expression (green; indicated by white arrows) which is not observed in wild-type (I). All confocal images were taken with a 40× water objective lens. Panels A–D are cryosections; panels E–L are plastic sections. Nuclei (blue) are stained with either DRAQ5 (A–D) or Hoechst (E–L). ZO-1 staining basal to the pronephros comes from a different tissue (asterisks in panels K and L) and does not reflect an alteration in ZO-1 within the pronephros.

30 hpf by taking video recordings of cilia movement (Materials and methods, Supplementary Data). In wild-type embryos, pronephric cilia are motile at 26 hpf, but they do not appear to bundle or show the coordinated cilia movement seen in our recordings at 2 and 3 dpf (Supplementary Videos 1–3). Cilia motility was evident from the cloaca region to the medial part of the kidney (data not shown). Analysis of more anterior cilia is not possible because the yolk obstructs imaging. At 26–30 hpf, *locke* mutants had motile cilia that exhibited a quick flickering movement, but with a reduced range of motion compared to wild-type (Supplementary Video 4). In contrast to *locke* mutants, *swt* mutants displayed completely immotile cilia (Supplementary Video 5). *kurly* mutants have plieotropic cilia motility phenotypes ranging from immotile cilia to cilia that are motile but beat irregularly (Supplementary Video 6). Cilia were also examined at these early stages by immunostaining with acetylated tubulin. Although *swt* and *kurly* mutants showed grossly normal lengths of cilia, *locke* mutants had shortened cilia (Figs. 5A–D). Our results on cilia length in *locke* are in agreement with those recently published (Zhao and Malicki, 2007).

The cilia motility phenotypes observed in *locke* and *swt* mutants at 26–30 hpf remain consistent at 2 dpf and 3 dpf (Supplementary Videos 7 and 8 and data not shown). Interestingly, we found that *kurly* mutants at 2 dpf had some cilia that bundled and moved similar to wild-type (Supplementary Videos 2 and 9). To more accurately compare the cilia motility in *kurly* mutants to that observed in wild-type embryos, we developed a method to determine the frequency of cilia movement at high precision by collecting and measuring scattered infra-red light (see Materials and methods). Through this analysis, we determined that both wild-type and *kurly* mutant ciliary bundles move at approximately 42 beats/s (Hz) at 48–52 hpf (Figs. 5K, L). This is in contrast to the previously determined frequency of 20 Hz obtained by counting cilia beats at a later time point (60 hpf) by Kramer-Zucker et al. (2005). The infra-red recording technique could not be applied to *swt* or *locke* embryos because the mutants never formed ciliary bundles and the amount of light scattered by a single cilium was too low to detect. Importantly, the cystic phenotypes we observed in all three mutants are similar despite each mutant having striking differences in cilia motility.

swt encodes a novel leucine rich repeat containing protein (LRRC50) that is required for ciliary motility in zebrafish

To better understand how these gene products are affecting cilia motility and cyst formation, it will be important to determine the molecular nature of the affected genes. To this end, we have cloned *swt* and find it encodes a novel leucine rich repeat containing protein (*lrrc50*; Fig. 7). LRRC50 in zebrafish is a 562 amino acid protein with a predicted molecular weight of 63 kDa. This protein contains six leucine rich repeats (LRR) at the N-terminus followed by a leucine cap domain and a coiled-coil domain. These domains are proposed to function as protein–protein interaction domains; however, the function of

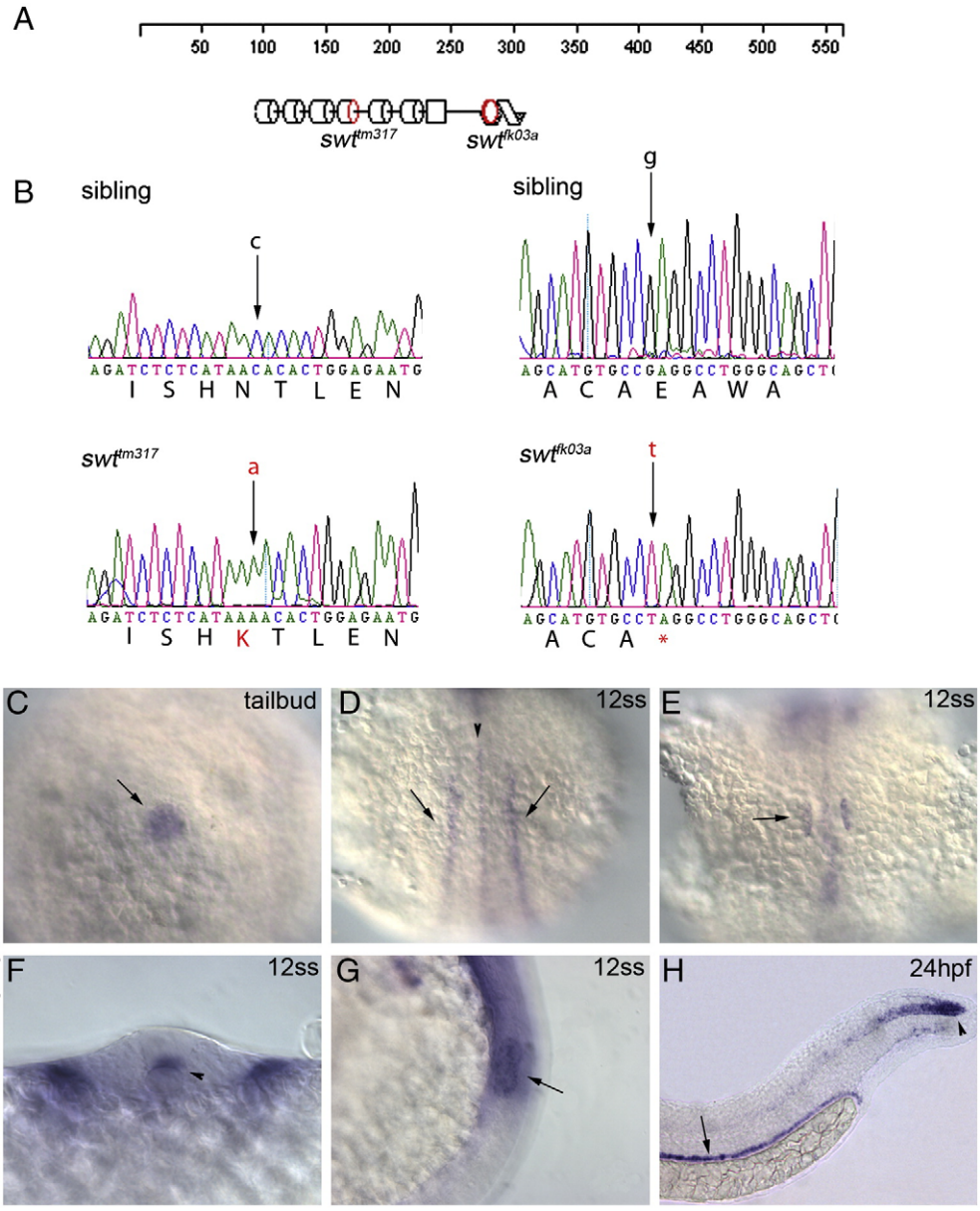

Fig. 7. *swt* encodes *lrrc50*, a novel gene required for cilia motility. (A) Schematic diagram of the LRRC50 protein highlighting the location of *tm317* and *fk03a* mutations. LRRC50 contains 6 predicted leucine rich repeats (cylinders), followed by a coiled-coil domain (spiral); however, the functions of these motifs in Swt are unknown. (B) Sequence traces of wild-type sibling and mutant DNA, showing the mutations in each allele. The swt^{tm317} allele creates a missense mutation changing AAC (ASN) to AAA (LYS) at amino acid position 172 in the leucine rich repeat region. The swt^{fk03a} allele creates a nonsense mutation changing GAG (GLU) to TAG (stop codon) at amino acid position 259 after the leucine rich repeats before the coiled-coil domain. *swt* RNA is expressed in cells that contain cilia: (C) Kupffer's vesicle (arrow); (D) neural tube staining (arrowhead) and bilateral intermediate mesoderm staining (arrows); (E) otic vesicle (arrow); (F) cross-section showing expression in the floorplate of the neural tube (arrowhead); (G) lateral view of otic vesicle expression (arrow); (H) pronephric duct (arrow, dorsal to the yolk extension) and chordo-neural hinge expression (arrowhead, at the tip of the tail). Embryo in panel C is at tailbud stage (dorsal view of posterior), panels D–G are at the 12 somite stage, and panel H is at 24 hpf. In panels D and E, anterior is up.

these motifs in *swt* is unknown. We have two alleles of *swt* which display similar pronephric cyst phenotypes and defects in left-right patterning (J.S.B and R.D.B. in preparation). A missense mutation in the swt^{tm317} allele changes an asparagine (AAC) to lysine (AAA) at amino acid position 172 within one of the leucine rich repeats (Figs. 7A, B). This mutation may affect the ability of the LRR domain to interact with appropriate targets. The second allele, swt^{fk03a}, creates a stop codon at position 259 which is predicted to truncate the protein before the coiled-coil domain (Figs. 7A, B). *lrrc50* is an ortholog to *ODA7*, a gene previously cloned in the green alga *Chlamydomonas* that was found to prevent axonemal outer row dynein assembly (Freshour et al., 2007; Kamiya, 1988). Mutations in *ODA7* were originally identified in *Chlamydomonas* by selecting for mutant strains showing reduced swimming velocity and reduced flagellar beat frequency. However unlike *swt* mutants, the cilia/flagella in *ODA7* mutants were not completely immotile (Kamiya, 1988). Based on a series of

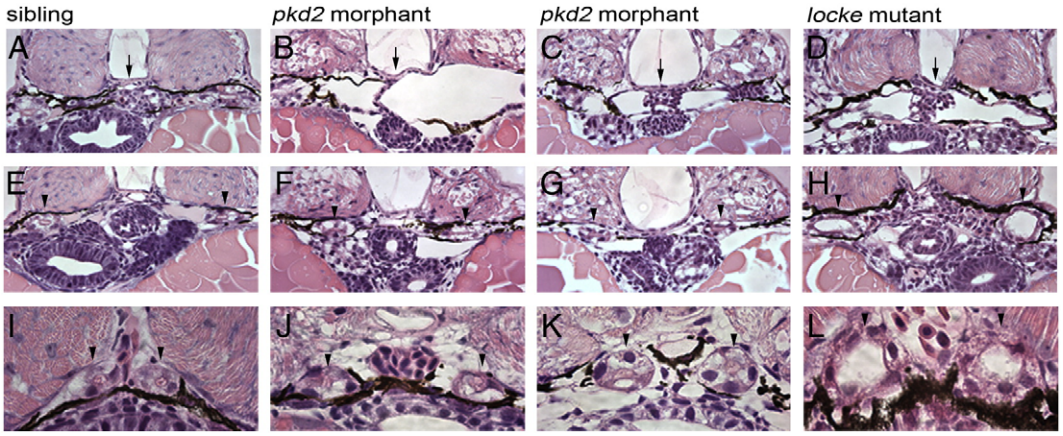

Fig. 8. *pkd2* morphants develop glomerular dilations, but do not become dilated in the tubular region of the nephron. (A–D) Glomerular region comparison at 3 dpf of a wild-type sibling embryo (A), *pkd2* morphants (B, C) and a *locke* mutant embryo (D). Black arrows mark the glomerulus, which is clearly dilated in both *pkd2* morphants and *locke* mutant embryos. (E–H) Anterior tubule region, immediately posterior to the glomerulus; although the tubules exhibit dilation in *locke* mutant embryos (H), the tubules in *pkd2* morphants (F, G) are not enlarged and resemble wild-type sibling tubules (E). (I–L) Medial tubule region; unlike *locke* mutant embryos (L), the lumens of the medial tubules are not dilated in *pkd2* morphants (J, K), similar to wild-type siblings (I). Black arrowheads indicate tubules. All pictures are from JB-4 plastic sections, stained with an H&E dye, and taken with 40× lens (A–H) and 100× oil lens (I–L).

biochemical fractionation studies, Freshour et al. (2007) report that *ODA7* serves as a structural bridge between the outer and inner row dynein motors in the axoneme, suggesting a role for coordinating cilia motility. Because *swt* mutants show immotile cilia in the kidney and neural tube (Supplementary Videos 5 and 8, data not shown), we were interested to determine where the gene product was expressed. *swt* RNA is maternally deposited in the embryo, as shown by RT-PCR (data not shown). By RNA *in situ* analysis, we observed *swt* expression in Kupffer's vesicle at the tailbud stage (Fig. 7C). Kupffer's vesicle is analogous to the mouse node in terms of having a critical role in left–right patterning and possessing motile cilia (Bisgrove and Yost, 2006). At the 12 ss, the *swt* RNA expression is found in the floorplate of the neural tube, in the intermediate mesoderm that gives rise to the pronephros, and the otic vesicle (Figs. 7D–G). At 24 hpf, *swt* RNA is observed in the kidney tubules and in the neural tube concentrated at the chordo-neural hinge (Fig. 7H). Thus, *swt* RNA was found in multiple tissues that are known to have motile cilia, further demonstrating the role of LRRC50 in cilia motility.

Zebrafish pkd2 morphants develop glomerular dilations, but not tubule dilations

Mutations in *polycystic kidney disease2* (*pkd2*) are the second leading cause of ADPKD (Gabow, 1993). However, *pkd2* mutants in zebrafish do not develop any type of tubule dilations or kidney cysts (Schottenfeld et al., 2007). It has widely been reported that morpholinos to *pkd2* in zebrafish do cause kidney cysts (Bisgrove et al., 2005; Obara et al., 2006; Schottenfeld et al., 2007; Sun et al., 2004). Because *locke*, *swt* and *kurly* all displayed defects in cilia motility, we were interested if *pkd2* morphants also had defects in cilia motility. To test if cilia motility was affected in *pkd2* morphants, we examined renal cilia by video microscopy at 2 dpf (see Materials and methods). In agreement with previous data from Obara et al., we found that the cilia in the *pkd2* morphants beat in a similar coordinated fashion to wild-type cilia, indicating that cilia motility is not affected in *pkd2* morphants (data not shown). However, our results indicate that the defect observed in *pkd2* morphants is different than the cysts characterized in *locke*, *swt* and *kurly* mutants. *pkd2* morphants develop glomerular dilations similar to *locke* mutants at 3 dpf (Figs. 8A–D), but the tubules and ducts never become dilated. Figs. 8E–H depict the anterior tubule region, which is slightly posterior to the glomerulus, where organs such as the gut, swim bladder and liver are apparent. Although the tubules are clearly dilated in *locke* mutant embryos (Fig. 8H) the tubules in *pkd2* morphants are similar in size to wild-type embryos (Figs. 8E–G). This phenotype is further evident in the medial region of the tubule (Figs. 8I–L). These data demonstrate that the *pkd2* morphants have glomerular dilations, but morphologically do not develop the same dilations observed in the other three genetic backgrounds with cilia motility defects. This suggests that there are different mechanisms involved in generating pronephric dilations.

Discussion

Utilizing zebrafish phenotypes to provide insights into human cystic diseases

One of the most powerful aspects of using zebrafish to understand human disease is the ability to perform detailed analyses to determine the first relevant phenotypes that occur. This is especially important in complex diseases such as PKD, where a network of cellular phenotypes has been detailed in the disease process, but the primary causes versus secondary consequences have not been elucidated. Based on our histological and cellular analysis, we present a model of when and where relevant phenotypes occur during cyst formation in zebrafish (Fig. 9). The first phenotypes we observe affect cilia motility (discussed below). We find that

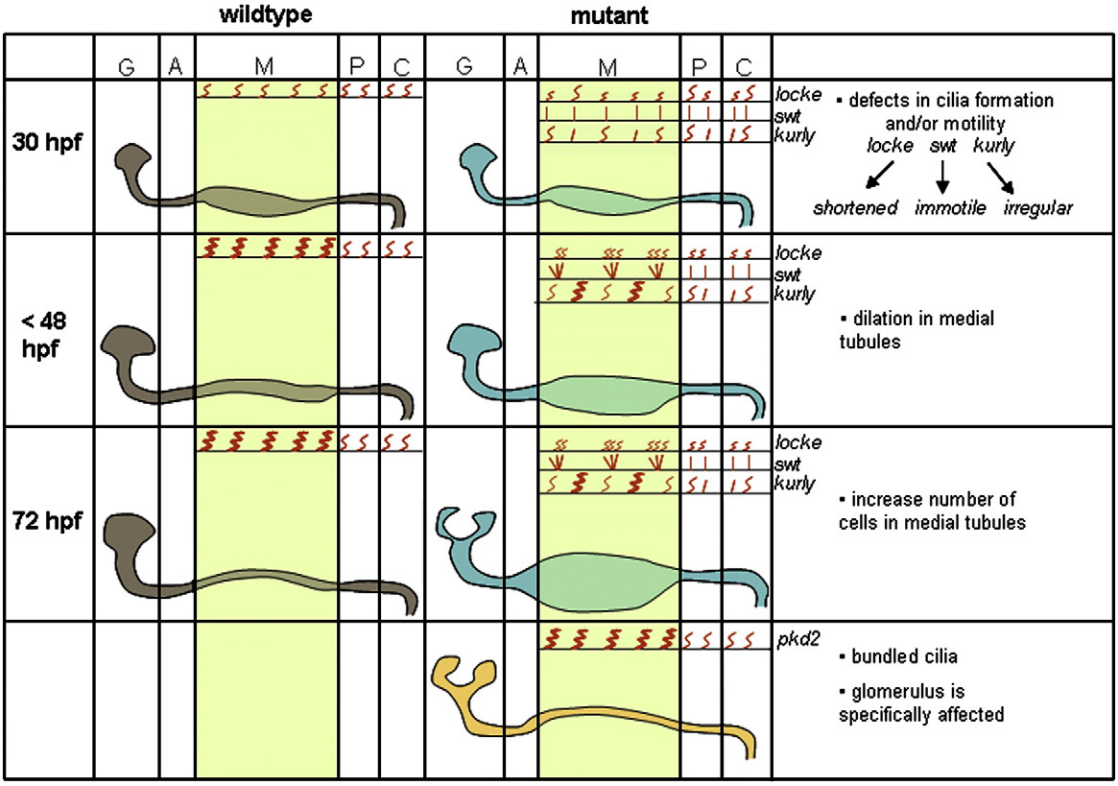

Fig. 9. Formation of pronephric cysts in zebrafish mutant embryos. In this model, longitudinal views of the pronephros along the anterior-posterior axis (left to right) are depicted and labeled. The 5 regions of interest are G=glomerulus, A=anterior tubule, M=medial tubule, P=posterior tubule, C=cloaca. At 30 hpf, the nephrons of both wild-type siblings (gray) and mutant (blue) embryos appear similar. At this stage, the cilia (red lines) in wild-type embryos are motile, but do not bundle. The mutant embryos each exhibit their own unique cilia motility defects at this stage. At 48 hpf, cells in the wild-type sibling medial tubules are multi-ciliated and the cilia have begun to bundle and move in a coordinated fashion. Cells in the posterior and cloaca regions contain monocilia which are motile as well. It is at the medial tubules where the cystic dilations begin in the mutant embryos. Although the medial tubules are drastically dilated in mutants, the lumens in the posterior and cloaca regions are similar in size to wild-type siblings. At 72 hpf, the medial tubules in the mutant embryos continue to dilate, while the wild-type sibling medial tubules decrease in size. At this stage, the anterior tubule and glomerular region of the mutant embryos are affected. The *pkd2* morphants (yellow) display cystic dilations specifically in the glomerulus. The medial tubule in *pkd2* morphants does not dilate and shows normal cilia motility. The highlighted column depicts the medial tubules.

cystic dilations occur first in the medial tubules prior to 48 hpf, while glomerular dilations are not consistently observed until 2.5 dpf. This result is significant because it shows that cystic dilations in these mutants are initially occurring in the medial tubules, which share considerable homology to the proximal convoluted and straight tubules (Wingert et al., 2007). This location is important as it further underscores the homology between zebrafish cyst formation and human disease. For example, in ARPKD, the cysts have been shown to transiently arise from the proximal tubules, then over time predominantly affect the collecting ducts (Nakanishi et al., 2000). Furthermore, it has been shown that the glomerulus can become dilated in human renal cystic diseases and in mouse models of ADPKD as a secondary effect to the tubular dilation, similar to what we observed in zebrafish cystic dilations (Bernstein, 1993; Tanner et al., 2002).

Defects in cellular remodeling may contribute to cystic dilations in locke, swt and kurly mutants

Although cystic dilations have been characterized in zebrafish embryos, this is the first report to show an increase number of cells surrounding the tubules. Since cellular overproliferation is a phenotype known to be associated with human PKD, we counted the number of cells surrounding the tubular lumens in wild-type and in each mutant background. By performing this experiment, we made two interesting observations. First, we found that at 3 dpf, the cell number increases significantly in the mutant medial tubules compared to wild-type. However, we did not observe an increased number of cells in the medial tubules at 2 dpf, indicating that the increased cell number is not the initial cause of the cystic dilations. It should be noted that at 2 dpf, a few tubules in *locke* mutants did appear to have an increased number of cells compared to age matched siblings. However, in these mutant tubules, the lumens appeared larger than in mutants without a cell number increase. Therefore, we believe that increases in cell number likely occur soon after dilation begins and may be a direct consequence of cellular responses to dilation. The increase in cell number that was observed at 3 dpf continued to rise at 5 dpf. This result suggests that the cystic cells observed in *locke*, *swt* and *kurly* mutants may have an overproliferation phenotype secondary to the initial cause of dilation. In human PKD, cystogenesis is hallmarked by increased rates of both cell proliferation and

apoptosis (reviewed in (Simons and Walz, 2006) and upregulation of the ERK/B-RAF/MAPK due to increased cAMP levels (Yamaguchi et al., 2003). Currently, most therapeutic approaches directly target either regulation of cell cycle (CKD inhibitor roscovitine, EGFR tyrosine kinase inhibitors) or apoptotic events (mTOR inhibitor rapamycin; Ibraghimov-Beskrovnaya, 2007; Shillingford et al., 2006; reviewed in Torres and Harris, 2007). Given that *locke*, *swt* and *kurly* have an increased number of cells that surround the cystic lumens, it will be interesting to determine in further studies if these drugs reduce cyst size in zebrafish embryos.

Our second interesting observation is that the number of cells surrounding the wild-type medial tubule decreases from 2 dpf to 3 dpf, while the number of cells increases in the mutant tubules. This result suggests that the wild-type tubule is undergoing a reorganization process to extend the pronephros along the anterior to posterior axis and/or regulate the general size of lumen diameter. It has been shown recently that the lengthening of the renal tubule in mice is governed by a planar cell polarity process which orients the plane of mitotic division in parallel to the tubular axis (Fischer et al., 2006). These authors also found that this regulated mitotic orientation was significantly affected in murine polycystic kidney models (Fischer et al., 2006). It will be interesting to determine whether planar cell polarity processes regulate zebrafish pronephric development and if these processes are defective in *locke*, *swt* and *kurly* mutants.

The role of cilia in pronephric cyst formation

Although cystic dilations in *locke*, *swt* and *kurly* mutants appear to be occurring at similar time points and in similar locations, the cilia motility defects associated with each mutant are remarkably different. It has been suggested that cilia motility defects in zebrafish mutant embryos create a general back-up of fluid flow in the nephrons and that this is the primary cause of cystic dilations (Kramer-Zucker et al., 2005). Although fluid back-up may exaggerate the phenotypes, we believe that this hypothesis does not fully explain the observed cystic dilations in *locke*, *swt* and *kurly* mutants for the following reasons. First, the mutant embryos rarely become grossly edemic. This implies that the kidney is still functioning and fluid is exiting the body. We have preliminary data that suggest that when the cloaca does not open the embryos do not develop enlarged tubules, but do become grossly edemic. Second, *swt* and *kurly* display opposite cilia motility defects; *swt* have completely immotile cilia while *kurly* cilia are motile and can move at the same frequency as wild-type when bundled. However, both mutants develop pronephric cysts. Interestingly, in *swt* the size of the cysts under light microscopy varies significantly between mutant embryos even though these mutants showed the most consistent phenotype in cilia motility defects. These data lead us to hypothesize that the cilia in the pronephric tubules may have other functions in addition to moving fluid through the pronephric duct. Furthermore, because the cystic phenotype in *locke*, *swt* and *kurly* embryos is highly similar, this suggests that a common pathway is affected in these mutants. Like in mammalian systems, these cilia could have roles in mechanosensation and regulation of cell cycle. Further work exploring additional roles for zebrafish pronephric cilia is a future focus of our laboratory.

As a first step toward understanding how our mutants contribute to cilia motility and cyst formation, we have identified the gene product mutated in *swt. swt* encodes a novel leucine rich repeat containing protein (LRRC50) that may function in protein-protein interactions. This gene is the ortholog of the Oda7 gene in the green alga Chlamydomonas where it has been shown to function in outer dynein assembly in axoneme structure. Mutations in Oda7 result in slower swimming behavior and reduced flagella beat frequency. This is in contrast to the *swt* mutant where cilia are completely immotile. It will be interesting to determine if the axoneme structure is disrupted in *swt* mutants to determine if the function of Lrrc50 is conserved. We find that *swt* RNA is expressed in cells that contain motile cilia including Kupffer's vesicle, the neural tube, kidney and otic vesicle. In the kidney, *swt* is expressed along the entire length of the nephron and appears to be required there for cilia motility. This is supported by our findings that immotile cilia are observed in the *swt* mutants from the cloaca to the medial region of the nephron. It is interesting, however, that the dilations are not observed throughout the entire nephron as the more posterior and cloaca regions are unaffected. Thus it is likely that the medial tubule cells are more sensitive to the loss of *swt* function.

pkd2 morphants suggest an alternate mechanism for cyst formation

By providing a histological time course of pronephric cyst development, we were able to compare the cystic dilations observed in *pkd2* morphants with cysts in *locke*, *swt* and *kurly* mutants. Unlike *locke*, *swt* and *kurly*, *pkd2* morphants have motile pronephric cilia that beat similar to wild-type cilia. Interestingly, the *pkd2* morphants did not develop cysts analogous to the ciliary motility mutants, as the dilations appeared to be restricted to the glomerular region. Likewise, *pkd2* null mice develop a preponderance of glomerular cysts (Wu et al., 2000). Thus, the *pkd2* morphants in zebrafish are more similar to *pkd2* nulls in mice. This is in contrast to the mouse unstable $Pkd2^{WS25}$ allele that develops cysts in the distal nephron segments and is a more analogous model to human PKD (Wu et al., 2000). The observed glomerular dilations in *pkd2* morphants may indicate a function of *pkd2* specifically in the glomerulus or during the development of glomerular fated tissue. We note that in Obara et al. they report cystic dilations in *pkd2* morphants as residing in the glomerulus and tubules. However, Wingert et al. have recently redefined the area referred to as tubules in Obara et al. as the neck segments. Our definitions of anterior and medial tubules are in agreement with the regions designated as tubules by Wingert et al. which are distinct from the neck segments and glomerulus. It will be interesting to see if the phenotype induced by the morpholino in Obara et al. affects what we refer to as the anterior and medial tubules. Overall, the differences we observe between the *pkd2* morphants and the other three cystic mutants described in this

report suggest that there are alternate mechanisms for cyst formation in zebrafish.

By performing this detailed characterization of pronephric cystic dilations, we have shown that zebrafish mutants show similar phenotypes to mammalian cystic diseases, particularly ARPKD. Additionally, we have provided a framework for further examination of cystic mutants in zebrafish. Future studies in zebrafish will broaden our understanding of cyst formation as we continue to explore the primary cellular defects associated with cystic expansion and the roles for the cilium in these processes.

Acknowledgments

We thank Robert Geisler and Silke Geiger-Rudolph for the original bulked segregant analysis that placed *switch hitter* on chromosome 7, Bo Xu for assistance with Matlab and statistical analysis, David Tank for suggesting the method to measure cilia frequency, Heather McAllister for zebrafish care and the members of the Burdine lab for helpful discussions and reading of the manuscript. R.D.B. is the 44th Scholar of the Edward Mallinckrodt Jr. Foundation, and funds from this award were used in support of this work. Funds from awards to R.D.B. from the New Jersey Commission on Cancer Research (04-2405-CCR-E0), the Polycystic Kidney Disease Foundation (#117b2r) and the National Institutes of Child Health and Human Development (1R01HD048584) were used in support of this work. J.S.B. is supported by predoctoral award 05-2411-CCR-E0 from the New Jersey Commission on Cancer Research. S.Y.T. and the Princeton Imaging facility are supported by NIH/NIGMS P50GM071508.

Appendix A. Supplementary data

Supplementary data associated with this article can be found, in the online version, at doi:10.1016/j.ydbio.2007.11.025.

References

The polycystic kidney disease 1 gene encodes a 14 kb transcript and lies within a duplicated region on chromosome 16. The European Polycystic Kidney Disease Consortium. Cell 78, 725.

Polycystic kidney disease: the complete structure of the PKD1 gene and its protein. The International Polycystic Kidney Disease Consortium. Cell 81, 289–298.

Avner, E.D., et al., 1992. Abnormal sodium pump distribution during renal tubulogenesis in congenital murine polycystic kidney disease. Proc. Natl. Acad. Sci. U. S. A. 89, 7447–7451.

Badano, J.L., et al., 2006. The Ciliopathies: an emerging class of human genetic disorders. Annu. Rev. Genomics Hum. Genet. 7, 125–148.

Baert, L., 1978. Hereditary polycystic kidney disease (adult form): a microdissection study of two cases at an early stage of the disease. Kidney Int. 13, 519–525.

Bernstein, J., 1993. Glomerulocystic kidney disease—nosological considerations. Pediatr. Nephrol. 7, 464–470.

Bisgrove, B.W., Yost, H.J., 2006. The roles of cilia in developmental disorders and disease. Development 133, 4131–4143.

Bisgrove, B.W., et al., 2005. Polaris and Polycystin-2 in dorsal forerunner cells and Kupffer's vesicle are required for specification of the zebrafish left–right axis. Dev. Biol. 287, 274–288.

Blacque, O.E., Leroux, M.R., 2006. Bardet–Biedl syndrome: an emerging pathomechanism of intracellular transport. Cell. Mol. Life Sci. 63, 2145–2161.

Brand, M., et al., 1996. Mutations affecting development of the midline and general body shape during zebrafish embryogenesis. Development 123, 129–142.

Brill, S.R., et al., 1996. Immunolocalization of ion transport proteins in human autosomal dominant polycystic kidney epithelial cells. Proc. Natl. Acad. Sci. U. S. A. 93, 10206–10211.

Burn, T.C., et al., 1995. Analysis of the genomic sequence for the autosomal dominant polycystic kidney disease (PKD1) gene predicts the presence of a leucine-rich repeat. The American PKD1 Consortium (APKD1 Consortium). Hum. Mol. Genet. 4, 575–582.

Drummond, I., 2003. Making a zebrafish kidney: a tale of two tubes. Trends Cell Biol. 13, 357–365.

Drummond, I.A., et al., 1998. Early development of the zebrafish pronephros and analysis of mutations affecting pronephric function. Development 125, 4655–4667.

Fischer, E., et al., 2006. Defective planar cell polarity in polycystic kidney disease. Nat. Genet. 38, 21–23.

Freshour, J., et al., 2007. Chlamydomonas flagellar outer row dynein assembly protein ODA7 interacts with both outer row and I1 inner row dyneins. J. Biol. Chem. 282, 5404–5412.

Gabow, P.A., 1993. Autosomal dominant polycystic kidney disease. N. Engl. J. Med. 329, 332–342.

Haffter, P., et al., 1996. The identification of genes with unique and essential functions in the development of the zebrafish, *Danio rerio*. Development 123, 1–36.

Hildebrandt, F., Zhou, W., 2007. Nephronophthisis-associated ciliopathies. J. Am. Soc. Nephrol. 18, 1855–1871.

Ibraghimov-Beskrovnaya, O., 2007. Targeting dysregulated cell cycle and apoptosis for polycystic kidney disease therapy. Cell Cycle 6, 776–779.

Kamiya, R., 1988. Mutations at twelve independent loci result in absence of outer dynein arms in *Chylamydomonas reinhardtii*. J. Cell Biol. 107, 2253–2258.

Kramer-Zucker, A.G., et al., 2005. Cilia-driven fluid flow in the zebrafish pronephros, brain and Kupffer's vesicle is required for normal organogenesis. Development 132, 1907–1921.

Lacy, E.R., et al., 1989. Flagellar cells and ciliary cells in the renal tubule of elasmobranchs. J. Exp. Zool., Suppl. 2, 186–192.

Liao, E.C., Zon, L.I., 1999. Simple sequence-length polymorphism analysis. Methods Cell Biol. 60, 181–183.

Liu, Y., et al., 2007. Notch signaling controls the differentiation of transporting epithelia and multiciliated cells in the zebrafish pronephros. Development 134, 1111–1122.

Ma, M., Jiang, Y.J., 2007. Jagged2a-notch signaling mediates cell fate choice in the zebrafish pronephric duct. PLoS Genet. 3, e18.

Menezes, L.F., Onuchic, L.F., 2006. Molecular and cellular pathogenesis of autosomal recessive polycystic kidney disease. Braz. J. Med. Biol. Res. 39, 1537–1548.

Nadasdy, T., et al., 1995. Proliferative activity of cyst epithelium in human renal cystic diseases. J. Am. Soc. Nephrol. 5, 1462–1468.

Nakanishi, K., et al., 2000. Proximal tubular cysts in fetal human autosomal recessive polycystic kidney disease. J. Am. Soc. Nephrol. 11, 760–763.

Obara, T., et al., 2006. Polycystin-2 immunolocalization and function in zebrafish. J. Am. Soc. Nephrol. 17, 2706–2718.

Omori, Y., Malicki, J., 2006. oko meduzy and related crumbs genes are determinants of apical cell features in the vertebrate embryo. Curr. Biol. 16, 945–957.

Ouchic, L.F., et al., 2002. PKHD1, the polycystic kidney and hepatic disease 1 gene, encodes a novel large protein containing multiple immunoglobulin-like plexin-transcription-factor domains and parallel beta-helix 1 repeats. Am. J. Hum. Genet. 70, 1305–1317.

Perrone, R.D., 1997. Extrarenal manifestations of ADPKD. Kidney Int. 51, 2022–2036.

Praetorius, H.A., Spring, K.R., 2001. Bending the MDCK cell primary cilium increases intracellular calcium. J. Membr. Biol. 184, 71–79.

Praetorius, H.A., et al., 2003. Bending the primary cilium opens Ca2+-sensitive intermediate-conductance K+ channels in MDCK cells. J. Membr. Biol. 191, 193–200.

Ramasubbu, K., et al., 1998. Increased epithelial cell proliferation and abnormal extracellular matrix in rat polycystic kidney disease. J. Am. Soc. Nephrol. 9, 937–945.

Schottenfeld, J., et al., 2007. Zebrafish curly up encodes a Pkd2 ortholog that restricts left-side-specific expression of southpaw. Development 134, 1605–1615.

Serluca, F.C., Fishman, M.C., 2001. Pre-pattern in the pronephric kidney field of zebrafish. Development 128, 2233–2241.

Shillingford, J.M., et al., 2006. The mTOR pathway is regulated by polycystin-1, and its inhibition reverses renal cystogenesis in polycystic kidney disease. Proc. Natl. Acad. Sci. U. S. A. 103, 5466–5471.

Simons, M., Walz, G., 2006. Polycystic kidney disease: cell division without a c(l)ue? Kidney Int. 70, 854–864.

Sun, Z., 2004. A genetic screen in zebrafish identifies cilia genes as a principal cause of cystic kidney. Development 131, 4085–4093.

Tanner, G.A., et al., 2002. Atubular glomeruli in a rat model of polycystic kidney disease. Kidney Int. 62, 1947–1957.

Thomson, R.B., et al., 2003. Histopathological analysis of renal cystic epithelia in the Pkd2WS25/-mouse model of ADPKD. Am. J. Physiol.: Renal Physiol. 285, F870–F880.

Torres, V.E., Harris, P.C., 2006. Mechanisms of disease: autosomal dominant and recessive polycystic kidney diseases. Nat. Clin. Pract. Nephrol. 2, 40–55.

Torres, V.E., Harris, P.C., 2007. Polycystic kidney disease: genes, proteins, animal models, disease mechanisms and therapeutic opportunities. J. Intern. Med. 261, 17–31.

Verani, R.R., Silva, F.G., 1988. Histogenesis of the renal cysts in adult (autosomal dominant) polycystic kidney disease: a histochemical study. Mod. Pathol. 1, 457–463.

Vize, P.D., et al., 1997. Model systems for the study of kidney development: use of the pronephros in the analysis of organ induction and patterning. Dev. Biol. 188, 189–204.

Ward, C.J., et al., 2002. The gene mutated in autosomal recessive polycystic kidney disease encodes a large, receptor-like protein. Nat. Genet. 30, 259–269.

Wilson, P.D., 2004. Polycystic kidney disease. N. Engl. J. Med. 350, 151–164.

Wilson, P.D., et al., 2000. Apical plasma membrane mispolarization of NaK-ATPase in polycystic kidney disease epithelia is associated with aberrant expression of the beta2 isoform. Am. J. Pathol. 156, 253–268.

Wingert, R.A., et al., 2007. The cdx genes and retinoic acid control the positioning and segmentation of the zebrafish pronephros. PLoS Genet. 3, 1922–1938.

Wu, G., et al., 2000. Cardiac defects and renal failure in mice with targeted mutations in Pkd2. Nat. Genet. 24, 75–78.

Yamaguchi, T., 2003. Cyclic AMP activates B-Raf and ERK in cyst epithelial cells from autosomal-dominant polycystic kidneys. Kidney Int. 63, 1983–1994.

Zerres, K., et al., 1998. Prenatal diagnosis of autosomal recessive polycystic kidney disease (ARPKD): molecular genetics, clinical experience, and fetal morphology. Am. J. Med. Genet. 76, 137–144.

Zhao, C., Malicki, J., 2007. Genetic defects of pronephric cilia in zebrafish. Mech. Dev. 124, 605–616.